



Graphene-Metal Hybrid Metamaterial for a Tunable Broadband Terahertz Linear-Polarization Conversion Switch and Linear-to-Circular Polarization

Xinwen Wang^{1,2} · Zhongyin Xiao^{1,2} · Xiang Miao^{1,2} · Xuxian Jiang^{1,2} · Anqi Li^{1,2}

Received: 8 December 2022 / Accepted: 16 January 2023 / Published online: 15 February 2023
© The Minerals, Metals & Materials Society 2023

Abstract

In this paper, we propose a tunable broadband terahertz (THz) linear polarization conversion switch (LPCS) and linear-to-circular polarization (LTCP) metamaterial. By tuning the Fermi energy level of graphene from $E_F = 0$ eV to $E_F = 1$ eV at 2.70–5.62 THz, it is possible to adjust the proposed structure from the linear polarization conversion (LPC) ON state to the LPC OFF state and also to tune the polarization conversion rate (PCR) from 1% to 99.99%. When $E_F = 0.5$ eV and is in the range of 5.56–5.96 THz, the structure can achieve LTCP function with ellipticity (η) exceeding 0.97 and an axial ratio (AR) of less than 1.5 dB. Based on the surface current and U-V decomposition, the LPC ON state, LPC OFF state and LTCP function are analyzed and well corroborated. Investigating graphene surface impedance at different fermi energy levels proves the polarization state tunable. The proposed structure can be applied to various fields of wireless communication, sensing and imaging.

Keywords Polarization conversion switch · graphene · metamaterial · linear-to-circular polarization

Introduction

Polarization, a significant property of electromagnetic waves, can increase the capacity of wireless communication by more than a few times.¹ Traditional polarization control is achieved by fiber grating or birefringent crystals.² However, these methods have complex phase accumulation processes that result in bulky equipment that is no longer suitable for today's practical needs. In recent years, metamaterials (MMs), as artificial electromagnetic mediums, have emerged as one of the best alternatives for polarization control because of their electromagnetic properties and ability to control electromagnetic waves without natural materials and the possibility of periodic alignment.^{3–5} In contrast to standard optical components, MMs, as artificial materials that

can be tailored to the electromagnetic response on demand, provide inspiring possibilities for high-density integration and miniaturization of terahertz (THz) devices.^{6–8} Polarization control of THz waves by periodically arranged MMs achieved fascinating results and have been widely applied in practice, such as coded metamaterials,^{9–11} near-field imaging,^{12,13} sensors,¹⁴ and wireless communication.¹⁵ However, most polarization control studies tend to be restricted to linear polarization conversion (LPC) and linear-to-circular polarization (LTCP) functions,^{16–18} and thus certain tunability is needed. Therefore, it is urgent to design a structure with a controllable polarization state and realize the LPC ON state, LPC OFF state and LTCP function. Moreover, the control method is simple and explicit.

In practical applications, devices designed from graphene have ideal tunability. Graphene is a hexagonal honeycomb lattice nanomaterial composed of carbon atoms,^{19,20} and by varying the chemical doping or gate voltage over a wide frequency range, the surface conductivity of graphene, which depends on the chemical potential, can be continuously varied.^{21,22} Because of its surface conductivity,²³ tunable optical transparency²⁴ and high electron mobility,²⁵ the control of the polarization state of THz waves has attracted widespread attention. For example, in 2020,

✉ Zhongyin Xiao
zhyxiao@shu.edu.cn

¹ School of Communication and Information Engineering, Key Laboratory of Specialty Fiber Optics and Optical Access Networks, Shanghai University, Shanghai, China

² School of Communication and Information Engineering, Shanghai Institute for Advanced Communication and Data Science, Shanghai University, Shanghai, China

Li et al. proposed a dynamically tunable THz broadband polarization converter. This structure dynamically converts linear polarization waves to cross-linear or circular polarization waves by graphene.²⁶ However, it needs more bandwidth to control polarization conversion and more tunability. In 2020, Zhang et al. proposed a switchable reflective THz polarization converter²⁷ that can modulate graphene's Fermi energy level to switch the linear polarization between quarter-wave and half-wave plates, enabling LPC and LTCP function. Nevertheless, the bandwidth is smaller and the polarization conversion efficiency could be higher. In 2021, Chen et al. designed a monolayer graphene broadband tunable reflective polarization converter that can convert linear co-polarized waves to cross-polarized waves with relatively flexible tuning of the bandwidth of the polarization conversion by adjusting the Fermi energy level of the graphene.²⁸ Yet its single function and tunability need to be improved. In 2022, Yuan et al. devised a graphene metamaterial-based tunable reflective THz polarization converter. By varying the Fermi energy level of graphene, the converter can achieve dual-band LPC and LTCP,²⁹ but its polarization conversion bandwidth needs more stability and comparatively lower bandwidth.

In this paper, we propose a tunable broadband THz linear polarization conversion switch (LPCS) and LTCP metamaterial. By tuning the Fermi energy level of graphene from $E_F = 0$ eV to $E_F = 1$ eV at 2.70–5.62 THz, it is feasible to adjust the proposed structure from LPC ON state to the LPC OFF state and also to tune the polarization conversion rate (PCR) from 1% to 99.99%. When $E_F = 0.5$ eV and in the range of 5.56–5.96 THz, the structure can achieve LTCP function with ellipticity (η) exceeding 0.97 and an axial ratio (AR) of less than 1.5 dB. Based on the surface current and U-V decomposition, the LPC ON state, LPC OFF state and LTCP function are analyzed and well corroborated. Investigating graphene surface impedance at different Fermi energy levels proves the polarization state tunable. Compared to the previously reported article, the proposed device has more functions and easily tunable and integrated features. We believe that the proposed structure has potential applications in tunable devices for THz communications.

Structural Design and Theory

The proposed reflective structure is shown in Fig. 1. Figure 1a shows that the structure consists of five layers: a double-graphene layer, a spacer layer, an I-type gold resonator, a dielectric layer and gold substrate. The double-graphene layer is a patterned sandwich structure consisting of two periodically patterned graphene layers and a Topas polymer ($\epsilon = 2.35$). Both spacer and dielectric layers are also constructed as Topas polymers, where the spacer is $t_1 = 0.1 \mu\text{m}$

and the dielectric layer is $d = 15 \mu\text{m}$. Figure 1b shows the double-graphene layer with opening size $P_3 = 14.6 \mu\text{m}$ and opening direction of -45° with respect to the x-axis. Figure 1c shows the I-type gold resonator placed in the x-axis direction with the following parameters: $P = 39 \mu\text{m}$, $l_1 = 23.4 \mu\text{m}$, $l_2 = 12.5 \mu\text{m}$, $w_1 = 4.3 \mu\text{m}$, $w_2 = 4.5 \mu\text{m}$, $t_2 = 0.1 \mu\text{m}$. As the gold film is perfectly reflective in the THz band, and its thickness has little effect on the performance of the structure, we set its thickness as $t = 1 \mu\text{m}$ to reduce the simulation time. The permittivity of gold follows the Drude model $\epsilon(\omega) = 1 - \omega_p^2/(\omega^2 + i\gamma\omega)$ with the plasma frequency $\omega_p = 1.37 \times 10^{16} \text{rad/s}$ and the damping constant is $\gamma = 4.07 \times 10^{13} \text{rad/s}$.

Graphene can be simulated as a 2D conductive surface impedance material,^{28,30,31} with surface impedance¹⁴ $Z_g = 1/\sigma_s$. In the THz band, the graphene surface complex conductivity can be expressed by the classical Kubo formula.³²

$$\sigma_{\text{intra}} = j \frac{e^2 k_B T}{\pi h^2 (\omega - j2\Gamma)} \left(\frac{E_F}{k_B T} + 2 \ln \left(e^{-\frac{E_F}{k_B T}} + 1 \right) \right) \quad (1)$$

$$\sigma_{\text{inter}} = \frac{j e^2}{4\pi h} \ln \left(\frac{2|E_F| - (\omega - j2\Gamma)h}{2|E_F| + (\omega - j2\Gamma)h} \right) \quad (2)$$

where σ_{intra} and σ_{inter} represent intraband and interband leap conductivity of graphene, respectively, ω is the angular frequency of the incident electromagnetic wave, E_F is the fermi energy level, e represents the charge of the electron, k_B denotes Boltzmann's constant. T indicates ambient temperature, h means approximate Planck constants. Γ indicates scattering rate, $\Gamma = 1/2\tau$, τ represents electron relaxation time. The Fermi energy level of graphene with applied bias voltage is expressed as^{16,22}:

$$E_F \approx hv_f \sqrt{\frac{\pi \epsilon_r \epsilon_0 V_g}{et_2}} \quad (3)$$

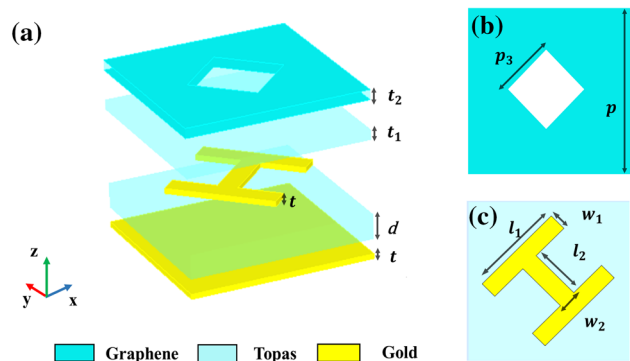


Fig. 1 (a) 3D model, (b) graphene layer, (c) I-type gold resonator.

Here, V_g is the bias voltage, ϵ_0 represents vacuum dielectric constant, and ϵ_r represents relative dielectric constant of the medium. t_2 is the thickness of the Topas polymer in the middle of the bilayer graphene pattern. $v_f = 1 \times 10^6 \text{ m/s}$ expresses the Fermi wave vector. Graphene's Fermi energy level E_F can be dynamically tuned from 0 eV to 1 eV.²¹ The rapidly developing micro and nano process technology provides methods for fabricating the proposed structures. First, a thin layer of Topas polymer is spin-coated on a silicon substrate, and a thick layer of Topas dielectric with the desired thickness is prepared by growing the spin-coated and cured layer using a thermal evaporation system.^{16,30} The I-type gold resonator is then designed using conventional optical techniques. Finally, bilayer graphene patterns are prepared in the Topas dielectric layer by repeated growth and transfer processes. Assuming ambient temperature $T = 300 \text{ K}$, $\tau = 0.6 \text{ ps}$, the higher relaxation time has easy tuning features, and in calculations, the single-layer graphene with a thickness of 0.34 nm is modeled as a 2D conductive layer.³¹ Using CST Microwave Studio 2020 for numerical simulations, the simulated results in this work were calculated by using the three-dimensional finite-difference time-domain (FDTD) method. In all simulations, period boundaries are applied in both x - and y -directions, and the perfectly matching layers are assigned along the z -direction. The incident THz waves are set to y -polarized TE mode employing the frequency domain solver.³³

In this paper, a reflective graphene-metal hybrid structure is proposed, and now we analyze the operating principles of the reflective graphene-metal hybrid structure from the theory. Assuming the incident electromagnetic wave propagates in the $-Z$ direction of linear polarization, the relationship between the incident linear component $\begin{pmatrix} E_x^i; E_y^i \end{pmatrix}$ and the reflected linear polarization component $\begin{pmatrix} E_x^r; E_y^r \end{pmatrix}$ can be expressed as¹²:

$$\begin{pmatrix} E_x^r \\ E_y^r \end{pmatrix} = \begin{pmatrix} r_{xx} & r_{xy} \\ r_{yx} & r_{yy} \end{pmatrix} \begin{pmatrix} E_x^i \\ E_y^i \end{pmatrix} = r \begin{pmatrix} E_x^i \\ E_y^i \end{pmatrix} \quad (4)$$

Here r_{xx} and r_{yy} are co-polarization transmission coefficients for linear polarization horizontal and vertical, respectively, r is the linear polarization of the Jones matrix. To better evaluate LPC performance, the PCR is introduced to describe the polarization conversion effectiveness¹⁸ and is defined as:

$$\text{PCR}(x) = \frac{|r_{yx}|^2}{|r_{xx}|^2 + |r_{yx}|^2} \quad (5)$$

$$\text{PCR}(y) = \frac{|r_{xy}|^2}{|r_{xy}|^2 + |r_{yy}|^2} \quad (6)$$

where $\text{PCR}(x)$ indicates the linear polarization horizontal polarization conversion efficiency and $\text{PCR}(y)$ indicates the vertical polarization conversion efficiency. Furthermore, for the measurement of the degree of LTCP, the η and AR are defined as follows²⁹:

$$\beta = \frac{1}{2} \sin^{-1} \left(\frac{2|r_{ii}||r_{ji}| \sin \Delta\varphi}{|r_{ii}|^2 + |r_{ji}|^2} \right) \quad (7)$$

$$\eta = \frac{2|r_{ii}||r_{ji}| \sin \Delta\varphi}{|r_{ii}|^2 + |r_{ji}|^2} \quad (8)$$

$$\text{AR} = 10 \times \log(\tan \beta) \quad (9)$$

where r_{ii} denotes co-polarization coefficient of the linear polarization, r_{ji} denotes cross-polarization coefficient of the linear polarization,⁴ and η and AR are used to evaluate the performance of circular polarization.³⁴ When $r_{ii} = r_{ij}$, that is $\text{PCR} = 0.5$, and $\Delta\varphi = \varphi_{ii} - \varphi_{ij} = \pi/2 + 2k\pi$ (k is an integer), at this time, AR is less than 3 dB, and the incident linear polarization wave can be converted into a circular polarization reflected wave. When η is $+1/-1$, the reflected wave is left-handed circular polarization (LHCP) wave/right-handed circular polarization (RHCP) wave, respectively.

Results and Discussion

Tunable Linear Polarization Transfer Switch Function

The structure of the proposed I-type gold resonator and double-graphene layer are symmetrically placed about the diagonal. The co-polarization and cross-polarization coefficients of the reflections are the same when the y -polarized and x -polarized waves are incident, so here we only use the case of the incident y -polarized waves for consideration. Figure 2a shows that at $E_F = 0 \text{ eV}$, from 2.70 THz to 5.62 THz, $|r_{xy}| > 0.55$, $|r_{yy}| < 0.25$, and in the range of 4.17–5.62 THz, $|r_{xy}| > 0.9$ and more extensive than $|r_{yy}|$. Figure 2b shows that PCR is greater than 90% from 2.70 THz to 5.62 THz and reaches the maximum value of 99.99% at 4.96 THz. At this point, the proposed structure acts as a linear polarization converter by the cross-polarization output; the LPC ON

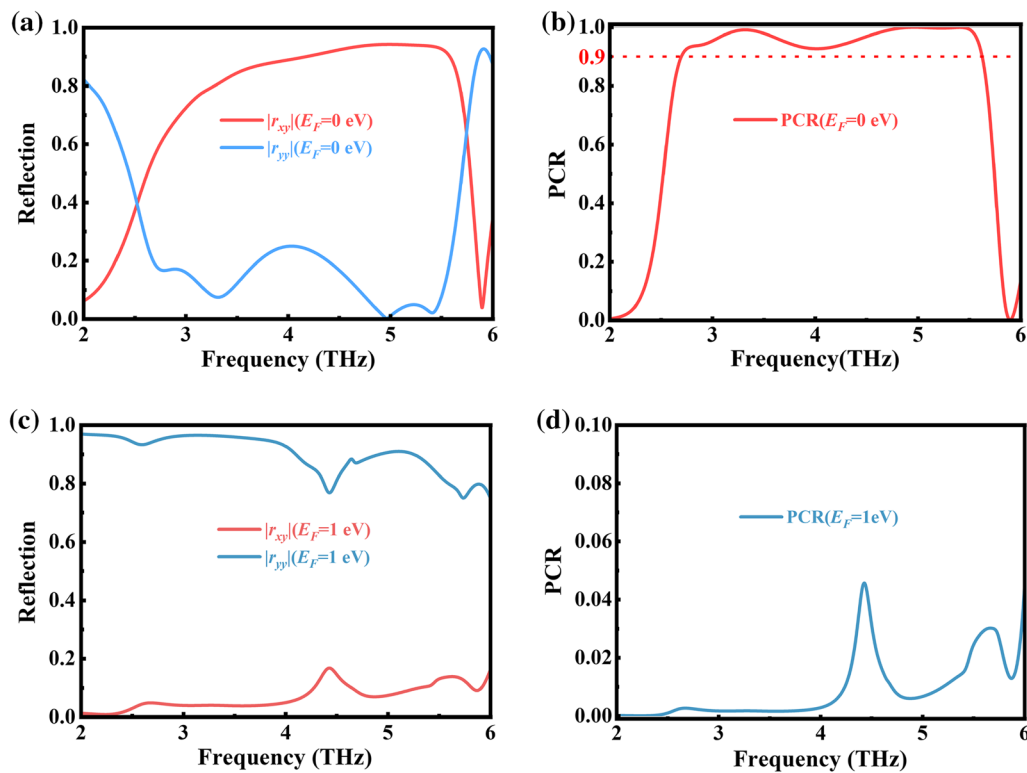


Fig. 2 (a) amplitude of the reflection coefficient at $E_F=0$ eV ($|r_{yy}|$ and $|r_{xy}|$), (b) PCR at $E_F=0$ eV, (c) amplitude of the reflection coefficient at $E_F=1$ eV ($|r_{yy}|$ and $|r_{xy}|$), (d) PCR at $E_F=1$ eV.

state can be achieved. Figure 2c shows that modulating the fermi energy level to $E_F = 1$ eV, in the range of 2.70 THz–5.62 THz, $|r_{yy}| > 0.77$, $|r_{xy}| < 0.16$. In this case, the output is by co-polarization. Figure 2d shows that PCR < 5% from 2.70 THz to 5.62 THz. It can achieve the LPC OFF state at this time. By tuning the Fermi energy level from 0 eV to 1 eV, PCR can be adjusted from 1% to 99.99%. Dynamically, the proposed structure acts as a broadband LPCS.

Tunable Linear-to-Circular Polarization

When the Fermi energy level is regulated to $E_F = 0.5$ eV, Fig. 3a shows that $|r_{xy}| = |r_{yy}| = 0.46 \sim 0.50$ and $\Delta\varphi = \varphi_{yy} - \varphi_{xy} = -90^\circ - 10^\circ/270^\circ - 10^\circ$ in the range of 5.56–5.96 THz. Figure 3b, c and d show that in this frequency band PCR = 0.5 ± 0.01 , ellipticity $\eta < -0.97$ and AR < 1.5dB < 3dB. To summarize, Fig. 3 explicitly illustrates the reflected rxy and ryy synthesized RHCP waves when y-polarized waves are incident on the structure at $E_F = 0.5$ eV in the range of 5.56–5.96 THz. As the proposed structure of the gold resonator and double graphene layers are symmetrically placed about the diagonal, the x-polarized waves at 5.56–5.96 THz are reflected by ryx and rxx

synthesized LHCP waves. It can achieve LTCP function at this time.

Physical Mechanism of the Polarization State

To analyze the LPC ON state's physical mechanism, we simulated the proposed structure's surface currents at 3.30 THz and 4.96 THz when $E_F = 0$ eV. Figure 4a, b and c show the surface currents distribution of the graphene layers, gold resonator and gold substrate at 3.30 THz. Graphene layers and the long arms of the I-type gold resonator together form inverse parallel currents with the gold substrate at low frequency. The reversed parallel currents form magnetic dipoles that produce a magnetic reaction, forming an induced magnetic field H_1 . While at 4.96 THz, the surface currents of graphene layers are relatively weakly distributed as shown in Fig. 4d, e and f, the currents on the short arm of the I-type gold resonator form homogeneous parallel currents with the currents on the gold substrate, leading to an electrical reaction that produces an induced electric field E. For the polarization conversion, the component H_{1y} of the induced magnetic field H_1 in the y-direction is parallel to the direction of the incident electric field E_i ; this ensures that cross-polarization coupling can be generated at low frequency. The component E_{1x} of the induced electric field

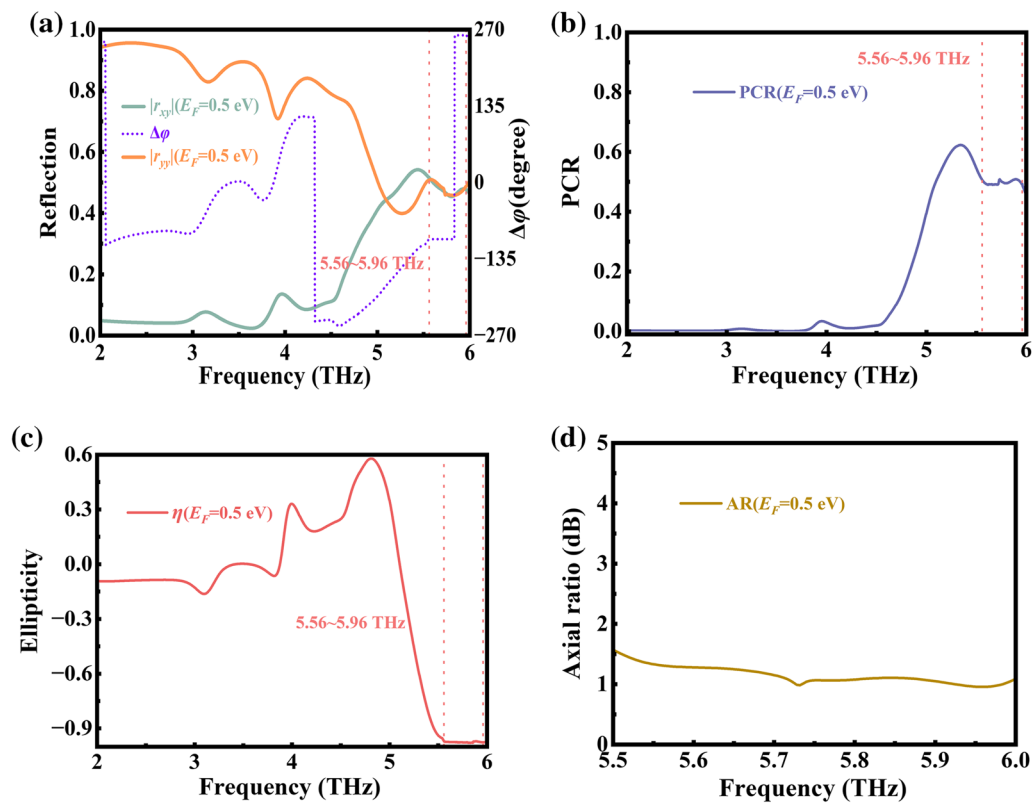


Fig. 3 (a) Amplitude of the reflection coefficient at $E_F = 0.5$ eV ($|r_{yy}|$ and $|r_{xy}|$) and phase difference value ($\Delta\phi$), (b) PCR at $E_F = 0.5$ eV, (c) ellipticity (η) at $E_F = 0.5$ eV, (d) axial ratio (AR) at $E_F = 0.5$ eV.

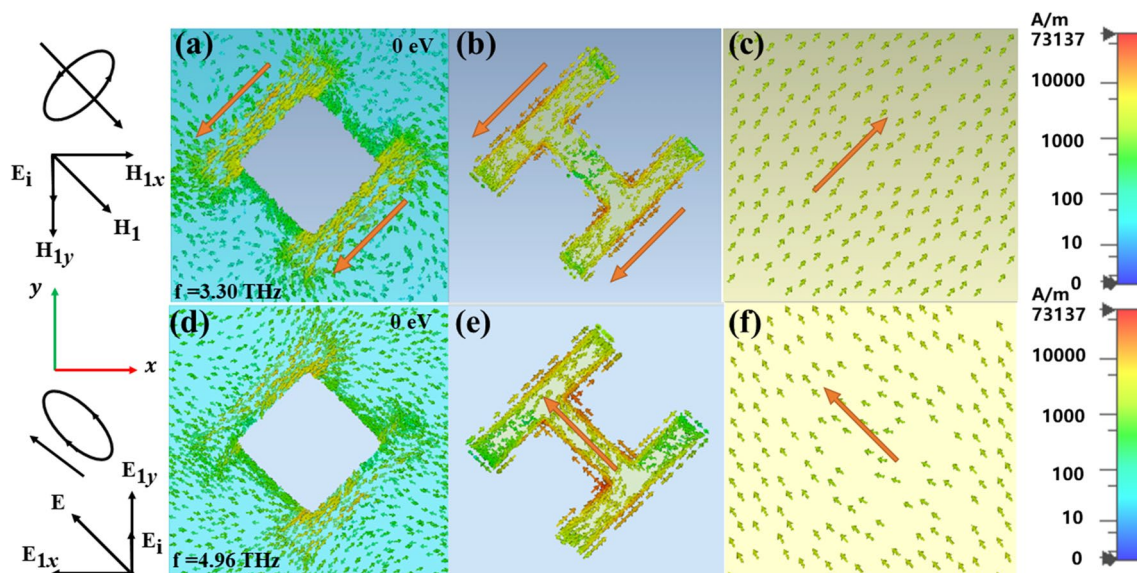


Fig. 4 (a), (b) and (c) surface currents of graphene layers, I-type gold resonator and gold substrate with $E_F = 0$ eV at 3.30 THz. (d), (e) and (f) surface currents graphene layers, I-type gold resonator and gold substrate with $E_F = 0$ eV at 3.30 THz.

E in the x -direction is perpendicular to the direction of the incident electric field E_i ; this ensures that cross-polarization coupling can be generated at high frequency, allowing cross-polarization to occur, so that y -polarized waves can be converted into x -polarized waves.

To analyze the reason for LPC OFF state, we also simulated the surface currents of the proposed structure at the points 3.30 THz and 4.96 THz when $E_F = 1$ eV. As shown in Fig. 5a, b and c, the graphene layers and the long arms of the I-type gold resonator at 3.30 THz have weak current strengths and cannot form reverse parallel currents with the gold substrate, thus failing to generate a magnetic resonance. Figure 5d, e and f shows the short arm of the I-type gold resonator with the gold substrate at 4.96 THz point, which could not form isotropic parallel currents at high frequency,

resulting in an electrical resonance. In summary, the proposed structure forms broadband LPC ON state at $E_F = 0$ eV and LPC OFF state at $E_F = 1$ eV.

To explain the physical mechanism of converting the reflected y -polarized waves into RHCP waves after incidence, we simulate the surface currents distribution at 5.65 THz when $E_F = 0.5$ eV. From the above, the high-frequency resonance point is mainly determined by the surface currents of the graphene layers independent of the surface currents of the graphene layers. Figure 6a, b, c and d shows the surface currents of the short arm of the I-type gold resonator at 5.65 THz, and Fig. 6a, b, c, and d show the I-type gold resonator short arm surface currents at 5.65 THz with 0° , 90° , 180° and 270° counterclockwise

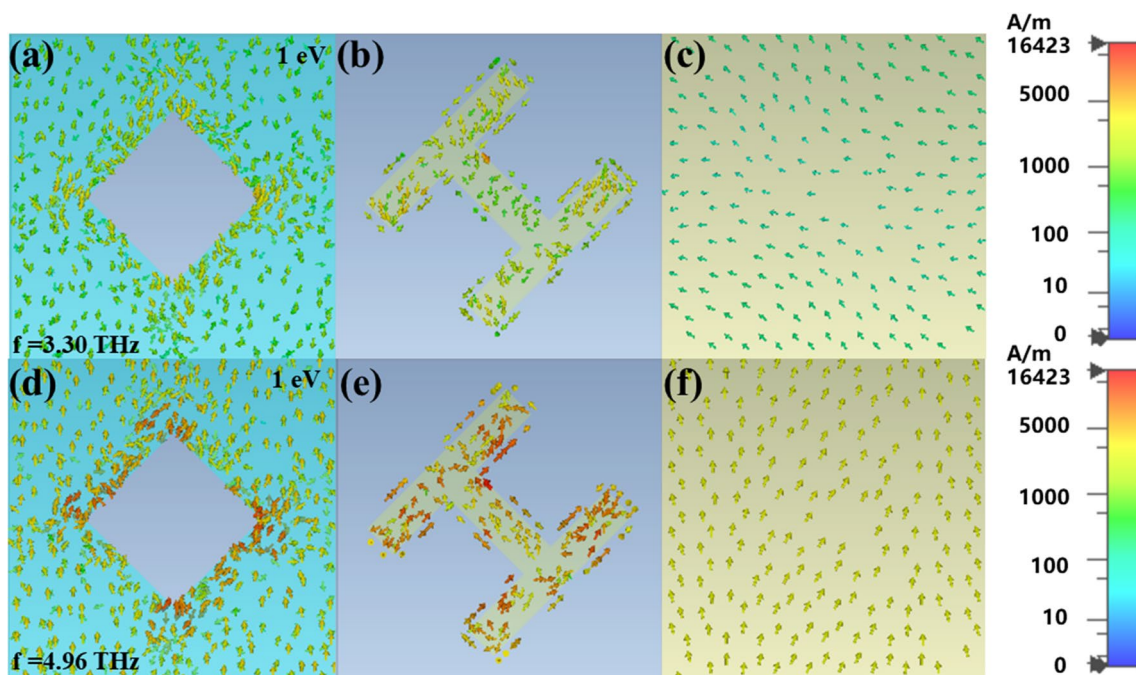


Fig. 5 (a), (b) and (c) surface currents of graphene layers, I-type gold resonator and gold substrate at 3.30 THz with $E_F = 1$ eV. (d), (e) and (f) surface currents of graphene layers, I-type metal resonator and metal substrate at 4.96 THz with $E_F = 1$ eV.

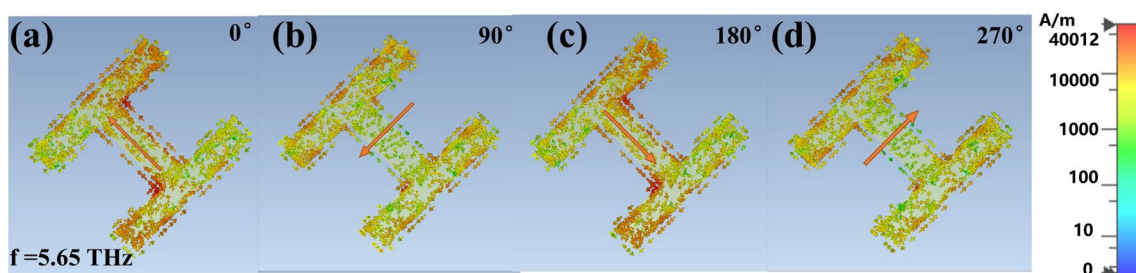


Fig. 6 (a), (b), (c) and (d) I-type gold resonator surface currents at 5.65 THz with 0° , 90° , 180° and 270° counterclockwise rotations when $E_F = 0.5$ eV.

rotations, indicating that the y -polarized waves are reflected to form the RHCP waves after incidence.

Suppose the electric field vector of the vertically incident electromagnetic wave along the MM is decomposed along the direction of the orthogonal coordinate axes. In that case, the polarization converter works as shown in Fig. 7a. The coordinate axis uOv is rotated by 45° from the coordinate axis xOy . According to the classical electromagnetic field theory, a phase difference of 0° indicates that the reflection is a co-polarized wave, a phase difference of $90^\circ/270^\circ$ signals that the reflection is a circularly polarized wave, and a phase difference of $\pm 180^\circ$ represents that the reflection is a cross-polarized wave. With the incident y -polarized wave as an example, Fig. 7b shows the phase response of the structure under E_u and E_v excitation at $E_F = 0$ eV. From 2.70 THz to 5.62 THz, the phase difference $\varphi_{uv} = \varphi_{vv} - \varphi_{uu} \approx \pm 180^\circ$, indicates that the structure achieves a broadband LPC ON state. According to Fig. 7c, at $E_F = 0.5$ eV from 5.56 THz to 5.96 THz, $\varphi_{uv} = \varphi_{vv} - \varphi_{uu} \approx 270^\circ$ indicates that the structure achieves LTCP function. According to Fig. 7d, at $E_F = 1$ eV from 2.70 THz to 5.62 THz, $\varphi_{uv} = \varphi_{vv} - \varphi_{uu} \approx 0^\circ$ indicates that the structure achieves a broadband LPC OFF state.

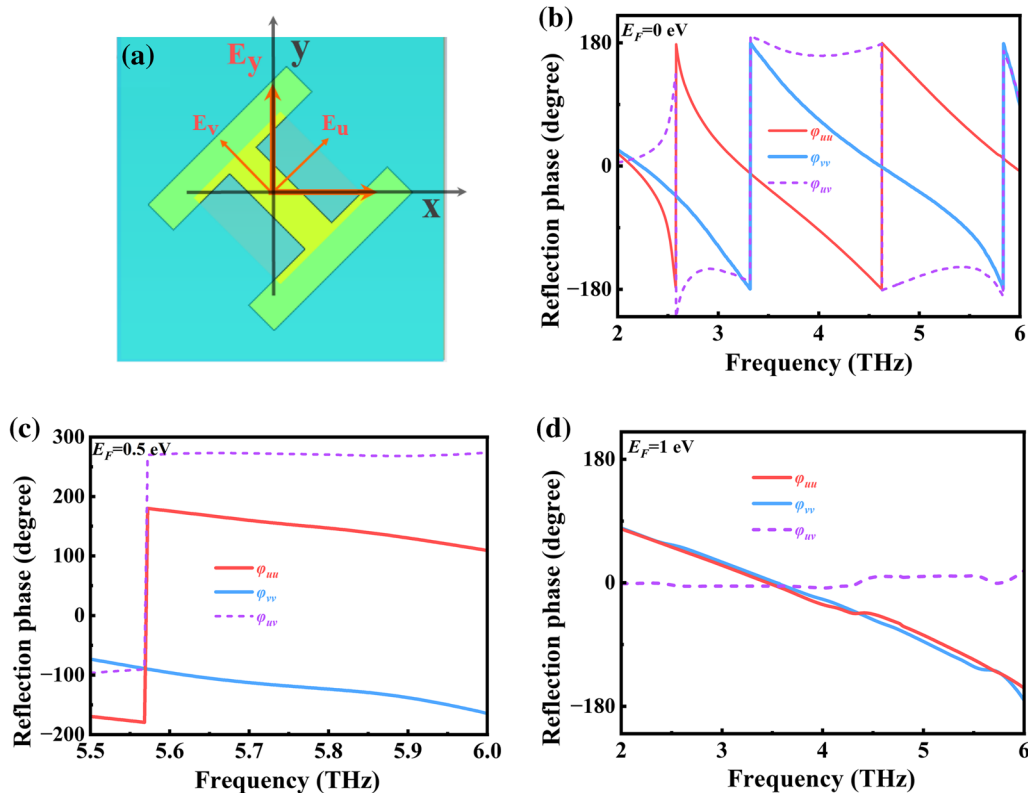
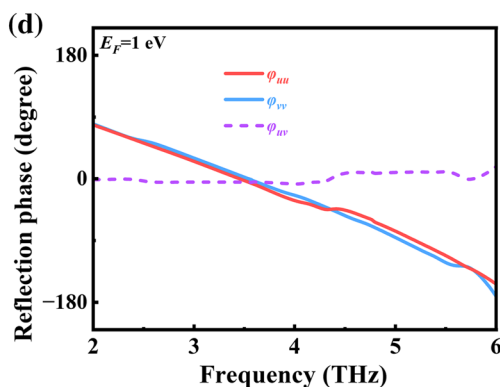
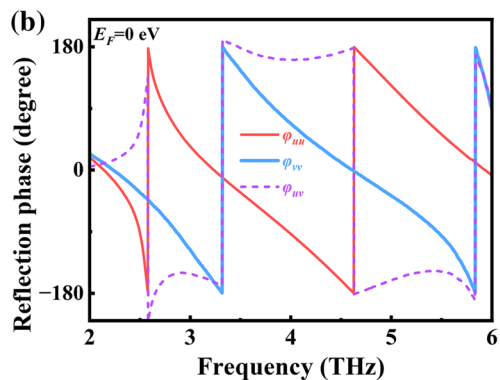


Fig. 7 (a) Electric field vector E_y decomposed into two orthogonal electric vectors E_u and E_v , (b) reflection phases (φ_{uu} and φ_{vv}) and phase difference (φ_{uv}) at $E_F = 0$ eV, (c) reflection phases (φ_{uu} and

We also elucidate the mechanism of the polarization state and analyze the polarization state of graphene at different fermi energy levels and its surface impedance. As shown in Fig. 8a, when $E_F = 0.05 \sim 0.20$ eV, as the Fermi energy level rises, the frequency band of the proposed structure with PCR $> 90\%$ decreases. Figure 8b and c shows the surface impedance of graphene $Z_g = 1/\sigma_s$, graphene surface impedance with $E_F = 0$ eV ranges from 465Ω at 2 THz to 2200Ω at 6 THz, when graphene is considered a dielectric film, it allows significant electromagnetic waves to be incident. While at $E_F = 0.05$ eV, surface impedance 260Ω to 530Ω , at $E_F = 0.10$ eV, $E_F = 0.15$ eV and $E_F = 0.20$ eV, surface impedance 145Ω , 94Ω and 70Ω . At this point, graphene gradually transitions from a dielectric film to a semi-metallic material, allowing a portion of the electromagnetic waves to be incident into the structure, producing the LPC ON state. For low frequency, the resonance point is mainly due to the action of the graphene layers and the long arms of gold resonator together with the gold substrate which produces magnetic resonance, while for high frequency, the resonance point is mainly due to the short arm of the gold resonator acting with the gold substrate to produce electrical resonance. Therefore, as the Fermi energy level of graphene rises, a blueshift of the low-frequency



φ_{vv}) and phase difference (φ_{uv}) at $E_F = 0.5$ eV, (d) reflection phases (φ_{uu} and φ_{vv}) and phase difference (φ_{uv}) at $E_F = 1$ eV.

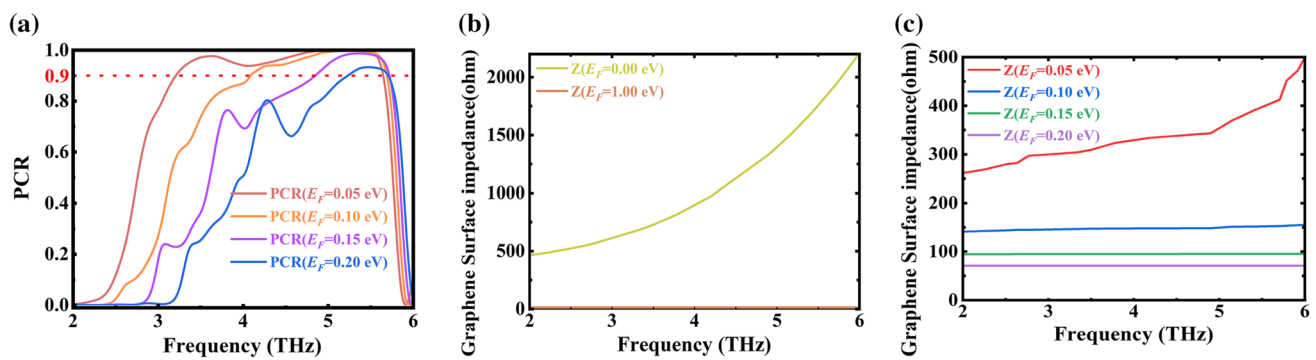


Fig. 8 (a) PCR with $E_F=0.05$ to 0.2 eV, (b) graphene surface impedance with $E_F=0$ eV and $E_F=1$ eV, (c) graphene surface impedance with $E_F=0.05$ to 0.2 eV.

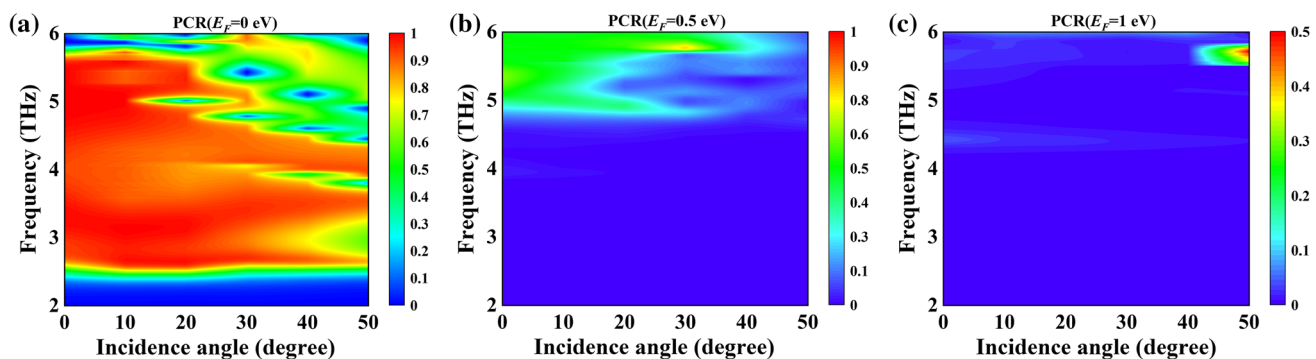


Fig. 9 (a) PCR with frequency and incidence angle at $E_F=0$ eV, (b) PCR with frequency and incidence angle at $E_F=0.5$ eV. PCR with frequency and incidence angle at $E_F=1$ eV.

resonance point occurs at $E_F = 0.05 \sim 0.20$ eV, while the high-frequency resonance point remains almost unchanged. When $E_F = 0.50$ eV with a graphene surface resistance of 28Ω , graphene layers transition from semi-metallic material to metallic material, and only a few electromagnetic waves are incident to the structure. At this time, the low-frequency resonance point does not exist, while the high-frequency resonance point will move down, resulting in LTCP function. At $E_F = 1$ eV, the graphene surface impedance of 14Ω is transformed to a metallic state, and many electromagnetic waves on the direct reflection will not produce a resonance point, thus playing a role in the LPC OFF state.

Figure 9 show the effect of PCR with frequency and incidence angle. The proposed structure at $E_F = 0$ eV shown in Fig. 9a maintains a stable bandwidth for incidence angles from 0° to 10° and decreases continuously as the incidence angle increases. Figure 9b shows the proposed structure at $E_F = 0.50$ eV, where the linear to circular polarization remains stable at an incidence angle of $0^\circ \sim 10^\circ$. Figure 9c shows the $E_F = 1$ eV, structure satisfies the LPC OFF state at an incidence angle of $0^\circ \sim 40^\circ$.

Finally, we compare some results with those of the devices reported in Table I for the graphene-based controlled polarization state THz simulation papers to demonstrate the innovation and performance of our proposed structure. In Table I, we list the functions, types, frequency ranges and bandwidths of the working implementations used in different studies. Table I shows that most studies focus on one or two modes of LPC and LTCP. Our proposed functional device can implement both LPC ON, LPC OFF state and LTCP function.

Conclusion

In this paper, we propose a device to dynamically control the polarization state of terahertz waves in the range of $2.70\text{--}5.62$ THz by tuning the Fermi level of graphene from $E_F = 0$ eV to $E_F = 1$ eV, which can adjust the proposed structure from the LPC ON state to the LPC OFF state, and the PCR can be tuned from 1% to 99.99%. When $E_F = 0.5$ eV and is in the range of $5.56\text{--}5.96$ THz, the structure can achieve LTCP function with η exceeding 0.97 and AR is less than 1.5 dB. We

Table 1 Comparison of previous THz simulation papers on graphene-based devices with controlled polarization states

References	Function	Type	Frequency range (THz)	Bandwidth (THz)
26	LPC	Dual function	2.24~2.74 THz	0.5
	LTCP		2.30~2.68 THz	0.38
27	LPC	Dual function	1.38~1.85 THz	0.47
	LTCP		1.38~1.72 THz	0.34
28	LPC	Single function	2.15~4.00 THz	1.85
29	LPC	Dual function	2.34~3.54, 3.38~4.43 THz	1.2, 1.05
	LTCP		2.14~2.62 THz	0.48
This work	LPC ON state	Triple function	2.70~5.62 THz	2.92
	LTCP		5.56~5.96 THz	0.40
	LPC OFF state		2.70~5.62 THz	2.92

simulated PCR at the Fermi level $E_F = 0 \sim 0.2$ eV, for which the structure is tunable for polarization conversion. Based on the surface current and U-V decomposition, the LPC ON state, LPC OFF state and LTCP function are analyzed and well corroborated. Investigating graphene surface impedance at different Fermi energy levels proves the polarization state tunable. We believe that the proposed structure has potential applications in tunable devices for THz communications.

Author Contributions XW: Conceptualization, Methodology, Software, Writing—Original Draft, Writing—Review Editing. ZX: Conceptualization, Validation, Writing—Review & Editing, Supervision. XM: Software, Data Curation. Writing—Review Editing. XJ: Software, Formal analysis. Investigation, Supervision. AL: Software, Investigation, Supervision.

Funding This study is supported by the National Natural Science Foundation of China (Grant No.61275070) and Natural Science Foundation of Shanghai (Grant No. 15ZR1415900).

Availability of Data and Materials All data generated or analyzed during this study are included in this published article.

Conflict of interest The authors declared that they have no conflicts of interest to this work. We declare that we do not have any commercial or associative interest that represents a conflict of interest in connection with the work submitted.

Consent for Publication Written informed consent for publication was obtained from all participants.

Consent to Participate Written informed consent for participation was obtained from all participants.

Ethical Approval We declare that this article is original, has not been published before, and is not currently considered for publication elsewhere. We confirm that the manuscript has been read and approved by all named authors and that there are no other persons who satisfied the

criteria for authorship but are not listed. We further confirm that the order of authors listed in the manuscript has been approved by all of us.

References

1. M.R. Andrews, P.P. Mitra, and R. DeCarvalho, Tripling the capacity of wireless communications using electromagnetic polarization. *Nature* 409, 316–318 (2001).
2. R. Magnusson, M. Shokooh-Saremi, and E.G. Johnson, Guided-mode resonant wave plates. *Opt. Lett.* 35, 2472 (2010).
3. P. Fei, G.A.E. Vandenbosch, W. Guo, X. Wen, D. Xiong, W. Hu, Q. Zheng, and X. Chen, Versatile cross-polarization conversion chiral metasurface for linear and circular polarizations. *Adv. Opt. Mater.* 8, 2000194 (2020).
4. H.X. Xu, S. Sun, S. Tang, S. Ma, Q. He, G.M. Wang, T. Cai, H.P. Li, and L. Zhou, Dynamical control on helicity of electromagnetic waves by tunable metasurfaces. *Sci. Rep.* 6, 27503 (2016).
5. H.-X. Xu, H. Liu, X. Ling, Y. Sun, and F. Yuan, Broadband vortex beam generation using multimode pancharatnam-berry metasurface. *IEEE Trans. Antennas Propag.* 65, 7378 (2017).
6. F. Ding, S. Zhong, and S.I. Bozhevolnyi, Vanadium dioxide integrated metasurfaces with switchable functionalities at terahertz frequencies. *Adv. Opt. Mater.* 6, 1701204 (2018).
7. J. Li, Y. Yang, J. Li, Y. Zhang, Z. Zhang, H. Zhao, F. Li, T. Tang, H. Dai, and J. Yao, All-optical switchable vanadium dioxide integrated coding metasurfaces for wavefront and polarization manipulation of terahertz beams. *Adv. Theory Simul.* 3, 1900183 (2019).
8. J. Li, Y. Zhang, J. Li, X. Yan, L. Liang, Z. Zhang, J. Huang, J. Li, Y. Yang, and J. Yao, Amplitude modulation of anomalously reflected terahertz beams using all-optical active pancharatnam-berry coding metasurfaces. *Nanoscale* 11, 5746 (2019).
9. F. Li, T. Tang, J. Li, L. Luo, C. Li, J. Shen, and J. Yao, Chiral coding metasurfaces with integrated vanadium dioxide for thermo-optic modulation of terahertz waves. *J. Alloys Compd.* 826, 154174 (2020).
10. J. Li, J. Li, Y. Zhang, J. Li, Y. Yang, H. Zhao, C. Zheng, J. Li, J. Huang, F. Li, T. Tang, and J. Yao, All-optical switchable terahertz

- spin-photonics devices based on vanadium dioxide integrated metasurfaces. *Opt. Commun.* 460, 124986 (2020).
11. J. Li, G. Wang, Z. Yue, J. Liu, J. Li, C. Zheng, Y. Zhang, Y. Zhang, and J. Yao, Dynamic phase assembled terahertz metalens for reversible conversion between linear polarization and arbitrary circular polarization. *Opto-Electron. Adv.* 5, 210062 (2022).
 12. J. Li, J. Li, C. Zheng, S. Wang, M. Li, H. Zhao, J. Li, Y. Zhang, and J. Yao, Dynamic control of reflective chiral terahertz metasurface with a new application developing in full grayscale near field imaging. *Carbon* 172, 189 (2021).
 13. J. Li, J. Li, Y. Yang, J. Li, Y. Zhang, L. Wu, Z. Zhang, M. Yang, C. Zheng, J. Li, J. Huang, F. Li, T. Tang, H. Dai, and J. Yao, Metal-graphene hybrid active chiral metasurfaces for dynamic terahertz wavefront modulation and near field imaging. *Carbon* 163, 34 (2020).
 14. J. Tian, R. Ke, R. Yang, and W. Pei, Tunable quad-band perfect metamaterial absorber on the basis of monolayer graphene pattern and its sensing application. *Results Phys.* 26, 104447 (2021).
 15. W. Xu, L. Xie, and Y. Ying, Mechanisms and applications of terahertz metamaterial sensing—a review. *Nanoscale* 9, 13864 (2017).
 16. Y. Zhang, Y. Feng, T. Jiang, J. Cao, J. Zhao, and B. Zhu, Tunable broadband polarization rotator in terahertz frequency based on graphene metamaterial. *Carbon* 133, 170 (2018).
 17. Z. Cui, Z. Xiao, M. Chen, F. Lv, and Q. Xu, All-dielectric transmission type three-frequency linearly polarized to circularly polarized converter. *Wave Random Complex.* (2021). <https://doi.org/10.1080/17455030.2021.1971324>.
 18. B. Tang and Y. Ren, Tunable and switchable multi-functional terahertz metamaterials based on a hybrid vanadium dioxide-graphene integrated configuration. *Phys. Chem. Chem. Phys.* 24, 8408 (2022).
 19. L. Qi, C. Liu, and S.M. Ali Shah, A broad dual-band switchable graphene-based terahertz metamaterial absorber. *Carbon* 153, 179 (2019).
 20. Y. Zhang, Y. Feng, and J. Zhao, Graphene-enabled active metamaterial for dynamical manipulation of terahertz reflection/transmission/absorption. *Phys. Lett. A* 384, 126840 (2020).
 21. W. Liu and Z. Song, Terahertz absorption modulator with largely tunable bandwidth and intensity. *Carbon* 174, 617 (2021).
 22. M. Zhang, and Z. Song, Switchable terahertz metamaterial absorber with broadband absorption and multiband absorption. *Opt. Express.* 29, 21551 (2021).
 23. L. Liu, W. Liu, and Z. Song, Ultra-broadband terahertz absorber based on a multilayer graphene metamaterial. *J. Appl. Phys.* 128, 093104 (2020).
 24. A. Andryieuski and A.V. Lavrinenko, Graphene metamaterials based tunable terahertz absorber: effective surface conductivity approach. *Opt. Express* 21, 9144 (2013).
 25. J. Qian, J. Zhou, Z. Zhu, Z. Ge, S. Wu, X. Liu, and J. Yi, Polarization-insensitive broadband THz absorber based on circular graphene patches. *Nanomaterials* 11, 2709 (2021).
 26. J. Li and R. Yang, Dynamically tuning polarizations of electromagnetic fields based on hybrid skew-resonator-graphene metasurfaces. *Opt. Express* 28, 4950 (2020).
 27. J. Zhang, K. Zhang, A. Cao, Y. Liu, and W. Kong, Bi-functional switchable broadband terahertz polarization converter based on a hybrid graphene-metal metasurface. *Opt. Express* 28, 26102 (2020).
 28. Y. Cheng, X. Zhu, J. Li, F. Chen, H. Luo, and L. Wu, Terahertz broadband tunable reflective cross-polarization convertor based on complementary cross-shaped graphene metasurface. *Phys. E* 134, 114893 (2021).
 29. X. Yuan, J. Chen, J. Wu, X. Yan, Y. Zhang, and X. Zhang, Graphene-based tunable linear and linear-to-circular polarization converters in the THz band. *Results Phys.* 37, 105571 (2022).
 30. Y. Zhang, Y. Feng, and J. Zhao, Graphene-enabled tunable multifunctional metamaterial for dynamical polarization manipulation of broadband terahertz wave. *Carbon* 163, 244 (2020).
 31. Y. Cheng and J. Wang, Tunable terahertz circular polarization convertor based on graphene metamaterial. *Diam. Relat. Mater.* 119, 108559 (2021).
 32. G.W. Hanson, Dyadic green's functions for an anisotropic, non-local model of biased graphene. *IEEE Trans. Antennas Propag.* 56, 747 (2008).
 33. Z. Peng, Z. Zheng, Z. Yu, H. Lan, M. Zhang, S. Wang, L. Li, H. Liang, and H. Su, Broadband absorption and polarization conversion switchable terahertz metamaterial device based on vanadium dioxide. *Opt. Laser Technol.* 157, 108723 (2023).
 34. X. Miao, Z. Xiao, Z. Cui, T. Zheng, and X. Wang, Ultra-wideband and multifunctional metamaterial polarization rotator in terahertz band. *Plasmonics* 17, 1379 (2022).

Publisher's Note Springer Nature remains neutral with regard to jurisdictional claims in published maps and institutional affiliations.

Springer Nature or its licensor (e.g. a society or other partner) holds exclusive rights to this article under a publishing agreement with the author(s) or other rightsholder(s); author self-archiving of the accepted manuscript version of this article is solely governed by the terms of such publishing agreement and applicable law.